Doctoral Dissertation

Studies on Novel Environmentally Friendly Inorganic Blue Pigments with Divalent Copper Ions as a Color Source

(二価銅イオンを発色源とする新規な環境調和型
青色無機顔料に関する研究)

SHIRAI Hiroaki

January 2022

Department of Applied Chemistry

Graduate School of Engineering

Osaka University

Preface

The study in this thesis has been carried out under direct supervision of Professor Dr. Nobuhito Imanaka at the Department of Applied Chemistry, Graduate School of Engineering, Osaka University.

The objective of this thesis is to develop novel environmentally friendly inorganic blue pigments by selecting a divalent copper ion as a color source and clarify the mechanism to enhance a blue color hue.

The author hopes that the results and findings obtained in this study contribute to the further development and systematization of novel environmentally friendly inorganic blue pigments and that the materials would make some profit for practical applications.

Hiroaki Shirai

Department of Applied Chemistry

Graduate School of Engineering,

Osaka University,

2-1 Yamadaoka, Suita,

Osaka 565-0871,

JAPAN January 2022

Contents

Chapter 3

Novel Environmentally Friendly Inorganic Blue Pigments Based on $Na_4Cu(PO_4)_2$

General Introduction

A pigment is opaque colored powder that is insoluble or hardly soluble in water, oil, alcohol, and/or other organic solvents. They color objects by sticking on the surface in the form of particles or by dispersing with a vehicle (dispersion media). The color of the pigment appears due to the selective absorption of specific visible light accompanying by electron transition such as *d*–*d* transition, charge transfer from ligands to metal (LMCT) or metal to ligands (MLCT), and band-gap transition, and we recognize its color as the complementary color to the absorbed light color. Table G1 lists the relationship between the absorbed light and complementary color. For example, when a material selectively absorbs light in the wavelength region at 580 to 595 nm corresponding to yellow light, it exhibits its complementary color of blue. In the field of pigments, we depict the color in terms of the CIE *L***a***b** color space in which all colors we recognize can be expressed (Figure G1). The parameter *L** indicates brightness or darkness on a neutral gray scale, and the parameters *a** (on the red (+) - green (−) axis) and *b** (on the yellow (+) - blue (−) axis) express color. By using these values, the chroma parameter (*C*) which shows color saturation and hue angle (*H*°) of a pigment are also estimated from the following equations; $C = [(a^*)^2 + (b^*)^2]^{1/2}$, $H° = \tan^{-1}(b^*/a^*)$. Here, the hue angle (*H*°) ranged from 0 to 360° and the value of pure red, yellow, and blue color is 0, 90, and 270°, respectively.

Table G1 The relationship between the absorbed light and complementary color

light	Purple	Blue	Green blue	Blue green	Green	Yellow green	Yellow	Orange	Red	Purple red
wavelength (nm)	380 ~ 435	435 ~ 480	480 ~ 490	490 ~ 500	500 ~ 560	560 ~ 580	580 ~ 595	595 ~ 605	605 ~ 750	750 ~ 780
complementary color	Yellow green	Yellow	Orange	Red	Purple red	Purple	Blue	Green blue	Blue green	Green

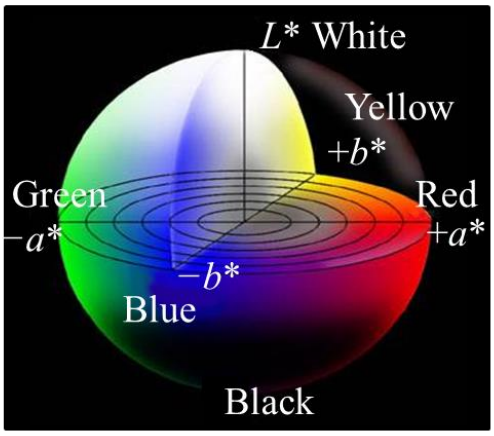

Fig. G1 CIE *L*a*b** color space.

Pigments are mainly classified into organic and inorganic ones. In general, there are wide variety of colors for the organic pigments whose vividness of colors are high, because the absorbed wavelength of visible light is easily controlled by modifying π conjugation in the molecule. However, many of organic pigments have critical problem that they cannot be used under harsh environments such as high temperature and UV-irradiated ones. On the other hand, inorganic pigments are inferior in vividness and abundance of colors compared with organic pigments, they possess the advantages of excellent thermal stability and UV light resistance and are widely applied in tiles, plastics, inks, and paints that are required to maintain their color for long periods [1, 2]. For decades, while various kinds of inorganic pigments have been used in industrial applications, most of them contain toxic heavy metals such as Cr, Co, Cd, and Pb, because these heavy metals exhibit strong and brilliant hues [1, 3-5]. However, the use of materials containing such heavy metals is becoming restricted owing to their harmful effect to both the human body and the earth environment. Therefore, it is necessary to develop alternative inorganic pigments that do not contain toxic heavy metals and many research groups have developed inorganic red [6-8], orange [9-14], yellow [15-21], green [22-25], and blue [26-29] pigments that meet the above condition.

Among the colors, there is a large demand for inorganic blue pigment because blue, one of the primary colors together with red and yellow, is an important color that gives people a refreshing

feeling. For the commercially available inorganic blue pigments, there are many compounds have been developed such as Co_2SiO_4, $CoAl_2O_4$, Co_2SnO_4, and $(Co, Zn)_2SiO_4$, whose color source is divalent Co^{2+} ions. Although vivid blue color can be obtained for these pigments due to the *d*–*d* transition of Co^{2+} [30], divalent Co^{2+} species are so harmful that the compounds containing Co^{2+} are designated as hazardous substances under the Pollutant Release and Transfer Register (PRTR) system and their use is restricted [30]. While there are some reports on the pigments whose Co^{2+} content is reduced to lower the bad effects of Co^{2+} [31-33], these pigments still contained a certain level of Co^{2+}, meaning that application of such pigments is not still suitable for realizing higher safety. As a non-toxic blue pigment, while iron cyanide, $Fe^{III}_4[Fe^{II}(CN)_6]_3$, is well known to show navy blue originated by the absorption of yellow light caused by the charge transfer between Fe^{2+} and Fe^{3+}, its blueness ($b^* = -19.3$) and color hue ($H° = 307.9$) in the CIE $L^*a^*b^*$ system and thermal stability (It gradually decomposes to iron oxide above 140 °C.) are insufficient for the use in paints and glazes. Therefore, it is demanded to develop novel inorganic blue pigments having a vivid color as well as high thermal and chemical stabilities without using any harmful elements. While it has been developed the $(Ca_{0.94}Eu_{0.06})_3Sc_2Si_3O_{12+\delta}$ solid whose color source was $Eu^{2+/3+}$ as an environmentally friendly inorganic blue pigment in our laboratory [34], vividness of blue color ($b^* = -33.8$, $H° = 307.1$) of this pigment was insufficient compared to commercially available cobalt blue ($CoAl_2O_4$: $b^* = -59.5$, $H° = 290.9$). Moreover, although other new environmentally friendly inorganic blue pigments have been developed as mentioned above [26-29], a vivid blue color has not yet been obtained.

Divalent copper ion, Cu^{2+}, is also expected to be a blue color source as same as Co^{2+}, $Fe^{2+/3+}$, and $Eu^{2+/3+}$ from the fact that various oxides containing Cu^{2+} show blue to green color by the absorption of the light other than these color in the spectrum by the charge transfer transition from O^{2-} to Cu^{2+} and the *d*–*d* transition of Cu^{2+} [35]. The alkaline earth metal silicates containing Cu^{2+} such as $CaCuSi_4O_{10}$ (Egyptian blue) and $BaCuSi_4O_{10}$ (Hans blue) have been used since ancient

period in time while the colors of these material are blue green [36, 37]. Moreover, $Sr_{0.7}La_{0.3}Cu_{0.7}Li_{0.3}Si_4O_{10}$ has been synthesized with relatively high blueness value ($b^* = -51.7$) [38]. While the blueness of this material is still low compared with cobalt blue ($CoAl_2O_4$: $b^* = -59.5$), divalent Cu^{2+} ion is expected to be an alternative candidate for blue color source because this blueness value is higher than those of above described harmless pigments, $Fe^{III}_4[Fe^{II}(CN)_6]_3$ or $(Ca_{0.94}Eu_{0.06})_3Sc_2Si_3O_{12+\delta}$.

In this research, I selected Cu^{2+} ions as a blue color source and developed novel environmentally friendly inorganic blue pigments composed of only nontoxic elements. To obtain vivid blue color, the charge transfer transition from O^{2-} to Cu^{2+} and the *d*–*d* transition of Cu^{2+} are intentionally controlled by modifying the Cu–O bond distance and/or O–Cu–O bond angle because the absorption of visible light is influenced by the coordination environment of Cu^{2+}. As a mother solid of blue pigments, I focused on $Ba(TiO)Cu_4(PO_4)_4$ and $Li_2Cu_5(PO_4)_4$ which contain planer CuO_4 units in the structures. Furthermore, the $Na_4Cu(PO_4)_2$ whose crystal structure has not been identified was also selected to clarify the possibility of Cu–O_x units as the origin of blue color.

This thesis consists of the following three chapters.

In Chapter 1, divalent Cu^{2+} site in the $Ba(TiO)Cu_4(PO_4)_4$ solid are partially replaced by Li^+ having larger ionic radius and lower valence state to intentionally distort the planer CuO_4 unit, and the color property of the $Ba(TiO)(Cu_{1-x}Li_x)_4(PO_4)_4$ solids are investigated with the discussion of relationship between distortion of CuO_4 unit and color.

In Chapter 2, Na^+ ions are introduced into the Li^+ sites of $Li_2Cu_5(PO_4)_4$ for the distortion of CuO_4 units, which does not cause the decrease in Cu^{2+} content in the solid, and the color of $(Li_{1-x}Na_x)_2Cu_5(PO_4)_4$ was investigated.

In Chapter 3, the effect of ionic size and electronegativity of the dopant on the color of pigment is investigated by doping Mg^{2+}, Ca^{2+}, or Zn^{2+} into the Cu^{2+} sites in the $Na_4Cu(PO_4)_2$ solid.

Chapter 1

Novel Environmentally Friendly Inorganic Blue Pigments Based on $Ba(TiO)Cu_4(PO_4)_4$

1.1 Introduction

As described in general introduction, there are some compounds that exhibit green to blue color for the inorganic materials containing Cu^{2+} due to the light absorption by the charge transfer transition from O^{2-} to Cu^{2+} and the *d*–*d* transition of Cu^{2+} [35]. In particular, since the compounds having square planar CuO_4 units in the structure often exhibits a green to blue color due to above two absorption [36], and are expected to be a candidate for the mother crystal of a novel environmentally friendly inorganic blue pigment while it is required to increase absorption of green color region.

In this chapter, I focus on $Ba(TiO)Cu_4(PO_4)_4$, which is composed of only harmless elements and has square planar CuO_4 units in the structure [39], as the mother crystal. Since the *d*–*d* transition of metal ions is generally influenced by their coordination environment, it is expected that the color of $Ba(TiO)Cu_4(PO_4)_4$ can be controlled by the intentional distortion of Cu^{2+} in the CuO_4 unit. Based on this concept, the Cu^{2+} (radius 0.057 nm, coordination number CN = 4) [40] site is partially replaced with Li^+ (radius 0.059 nm, CN = 4) [40] having a larger ionic radius and lower valence state in order to distort the CuO_4 units and, thereby, causes a shift of the absorption bands due to charge transfer and *d*–*d* transitions, and the color properties of the products are discussed.

1.2 Experimental procedure

The $Ba(TiO)(Cu_{1-x}Li_x)_4(PO_4)_4$ ($0 \leq x \leq 0.15$) solids were prepared by a conventional solid-state reaction method. Starting materials of $BaCO_3$, TiO_2, CuO, Li_2CO_3, and $(NH_4)_2HPO_4$ were mixed using an agate mortar, and the mixed powder was further mechanically mixed using a

planetary ball milling apparatus (P-7, FRITSCH) at 300 rpm for 1 h. For the samples other than $x = 0$, an excess amount of $BaCO_3$ (105% of the stoichiometric amount) was weighed for compensating the volatilization of Ba during the calcination step to obtain the single-phase samples. After the mixed powder was preheated at 600 °C for 6 h, the sample powders were calcined for 5 h in air atmosphere at 980 °C for $x = 0$ and at 900 °C for $x \geq 0.07$.

The crystal structures of the samples were identified by X-ray powder diffraction (XRD; SmartLab, Rigaku) with Cu Kα radiation (40 kV, 30 mA). The crystallographic data of the samples were calculated by Rietveld refinement using the RIETAN-FP program [41]. The optical reflectance spectra were recorded by a UV-visible spectrophotometer (UV-2600, Shimadzu) with barium sulfate as the reference. The color properties of the samples were obtained in terms of CIE $L^*a^*b^*$ system with a colorimeter (CR-400, Konica-Minolta).

Acid resistance was tested by dispersing the sample powder in a 4 wt% acetic acid aqueous solution. After stirring for 30 min, the sample was filtered, washed with deionized water and ethanol, and dried at room temperature. Thermal resistance test was performed by heating the sample at 900 °C for 24 h in atmospheric air. In addition, light resistance test was carried out under UV irradiation for 100 h using an UV lamp (EFD15BLB, Toshiba) with emission wavelength of 352 nm. The color differences of the pigments after each resistance tests were evaluated using the color parameters.

1.3 Results and discussion

Figure 1.1 shows the X-ray powder diffraction (XRD) patterns of the $Ba(TiO)(Cu_{1-x}Li_x)_4(PO_4)_4$ ($0 \leq x \leq 0.15$) samples. For the samples with $x \leq 0.10$, only diffraction peaks corresponding to a single-phase of tetragonal $Ba(TiO)Cu_4(PO_4)_4$ structure was observed, and no peaks for impurities were evident in the pattern. On the other hand, for the samples with $x \geq 0.13$, additional peaks of TiO_2 and $Cu_2P_2O_7$ were observed. In order to confirm the partial substitution of

Li^+ ions for Cu^{2+}, the lattice volumes of the $Ba(TiO)Cu_4(PO_4)_4$ phase in the samples were calculated from the XRD peak angles (Fig. 1.2). The lattice volume increased with increasing Li^+ content (x) up to 0.10, which suggests that Li^+ doped fully replaces Cu^{2+} sites in $Ba(TiO)Cu_4(PO_4)_4$, because the ionic radius of Li^+ (0.059 nm) [40] is larger than that of Cu^{2+} (0.057 nm) [40]. However, the lattice volumes were almost constant in the range where impurity phases appeared. This result strongly suggests that the samples with $x \leq 0.10$ successfully formed the single phase of solid solution.

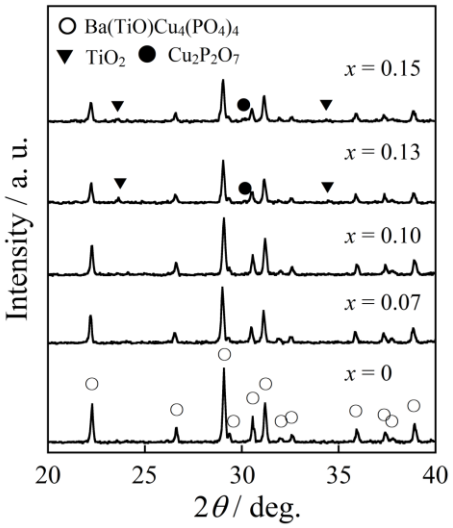

Fig. 1.1 XRD patterns of the $Ba(TiO)(Cu_{1-x}Li_x)_4(PO_4)_4$ samples.

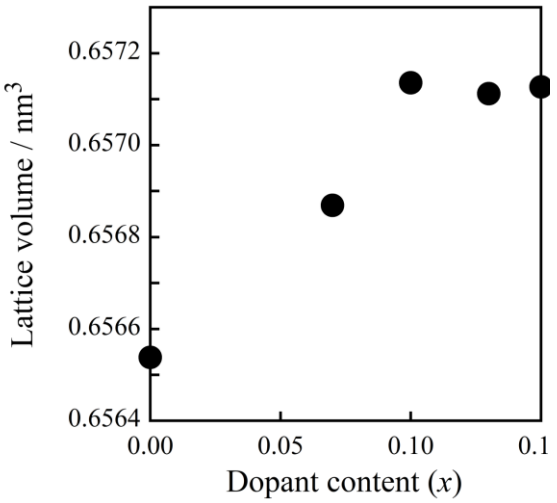

Fig. 1.2 Lattice volumes of the $Ba(TiO)(Cu_{1-x}Li_x)_4(PO_4)_4$ samples.

To investigate the effect of Li^+ substitution on the distortion of the CuO_4 units in the crystal structure, Rietveld refinement was conducted by the RIETAN-FP program [41] for the sample with $x \leq 0.10$ (Fig. 1.3). The observed patterns for all samples were assigned well by the tetragonal $Ba(TiO)Cu_4(PO_4)_4$ structure with the relatively small R_{wp} and S values. Figure 1.4 depicts the top and side view of the CuO_4 unit in the $Ba(TiO)(Cu_{0.90}Li_{0.10})_4(PO_4)_4$ solids estimated from the Rietveld refinement result. The O1–Cu–O4 and O2–Cu–O3 angles and Cu–O distances of the CuO_4 unit are tabulated in Table 1.1. It was confirmed that both the O1–Cu–O4 and O2–Cu–O3 angles monotonically decreased with increasing the Li^+ content, suggesting that the distortion of the CuO_4 is introduced by doping Li^+ into the Cu^{2+} site and degree of distortion is increased with x. This

distortion is considered to be a result of the partial replacement of Cu^{2+} by the monovalent Li^{+} ion with a larger ionic radius than Cu^{2+}; both the formation of oxygen vacancy and the difference in ionic radius should distort the O–Cu (Li)–O angles to stabilize the crystal structure. Moreover, Cu–O1 distance increased and Cu–O2, Cu–O3, and Cu–O4 distances decreased by doping Li^{+} into the Cu site, while the Cu–O4 distance of the solid with x = 0.10 was slightly larger than that for the sample with x = 0.07, probably due to the effect of the concentration of oxygen vacancy.

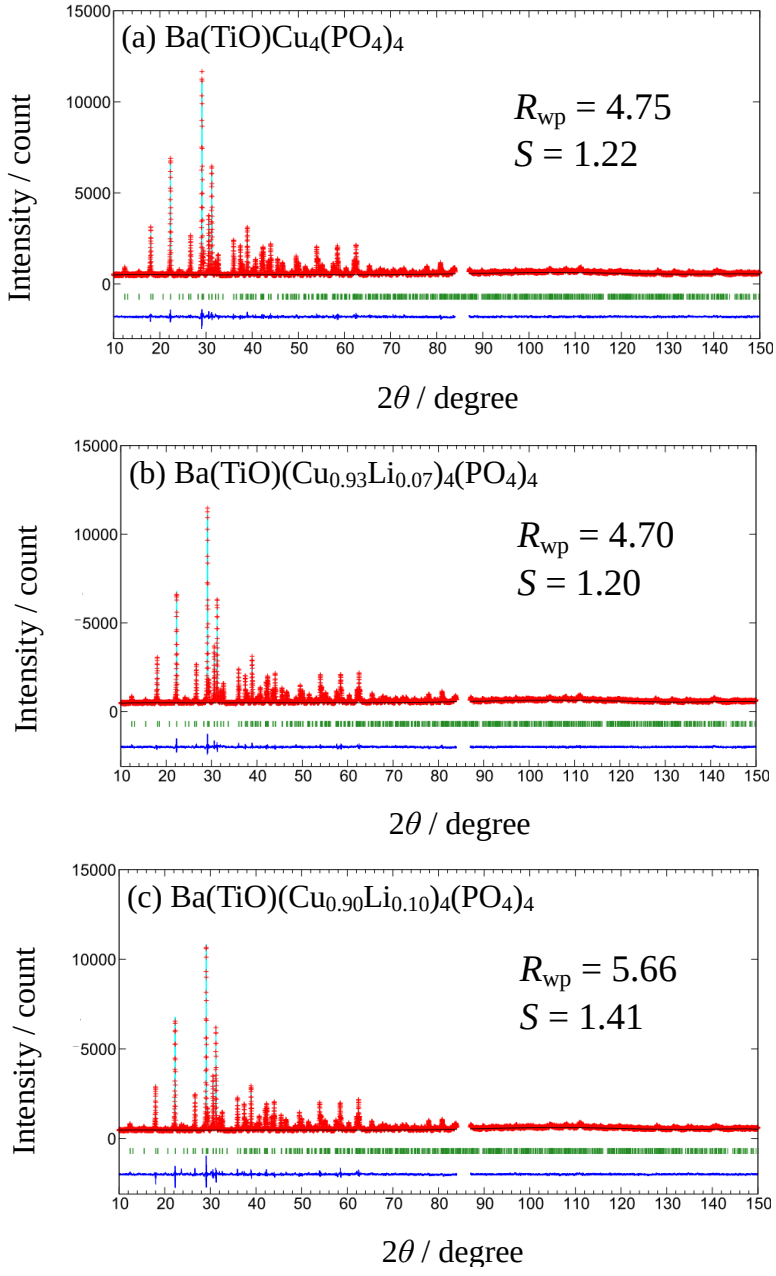

Fig. 1.3 Results of Rietveld refinement for (a) $Ba(TiO)Cu_4(PO_4)_4$, (b) $Ba(TiO)(Cu_{0.93}Li_{0.07})_4(PO_4)_4$, and (c) $Ba(TiO)(Cu_{0.90}Li_{0.10})_4(PO_4)_4$.

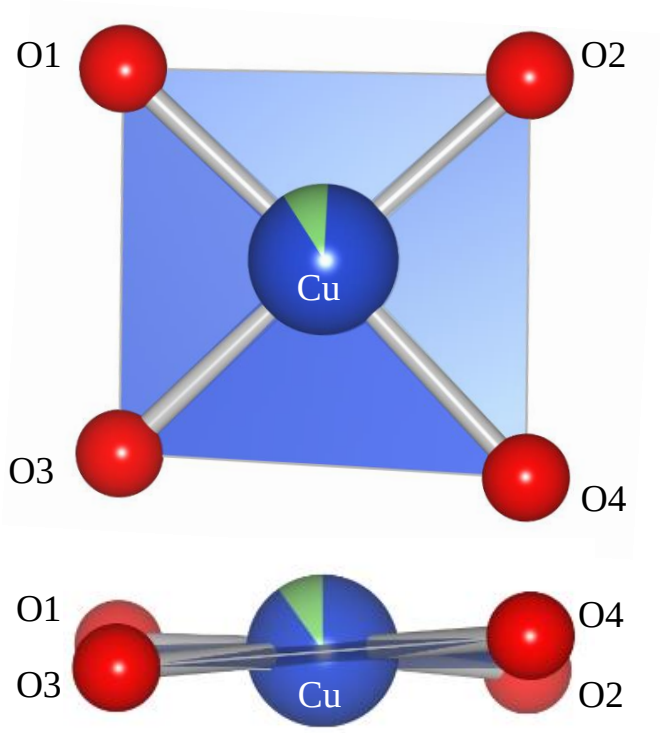

Fig 1.4 Schematic diagram of CuO_4 unit of the $Ba(TiO)(Cu_{0.90}Li_{0.10})_4(PO_4)_4$.

Table 1.1 O-Cu-O angles and Cu-O distances of CuO_4 unit of $Ba(TiO)(Cu_{1-x}Li_x)_4(PO_4)_4$ (x = 0, 0.07, 0.10)

Sample	O1-Cu-O4 / degree	O2-Cu-O3 / degree	Cu-O1 / Å	Cu-O2 / Å	Cu-O3 / Å	Cu-O4 / Å
$Ba(TiO)Cu_4(PO_4)_4$	177.78	175.43	1.977	1.958	1.986	1.874
$Ba(TiO)(Cu_{0.93}Li_{0.07})_4(PO_4)_4$	176.45	173.04	2.009	1.888	1.963	1.844
$Ba(TiO)(Cu_{0.90}Li_{0.10})_4(PO_4)_4$	174.64	172.56	2.015	1.860	1.915	1.866

Figure 1.5 displays the UV-vis diffuse reflectance spectra of the $Ba(TiO)(Cu_{1-x}Li_x)_4(PO_4)_4$ ($0 \leq x \leq 0.15$) samples. All samples exhibited two kinds of strong optical absorption at wavelengths shorter than and longer than ca. 470 nm, resulting in strong reflection between 400 to 550 nm which includes the blue region (435-480 nm). The optical absorptions at wavelengths shorter than 470 nm and those at wavelengths longer than 470 nm correspond to the charge transfer transition from O^{2-} to Cu^{2+} and to the *d–d* transition of Cu^{2+}, respectively [24]. For the samples with $x \leq 0.10$, the reflectance in the wavelength region of ca. 580 to 595 nm (yellow, which is the complementary color

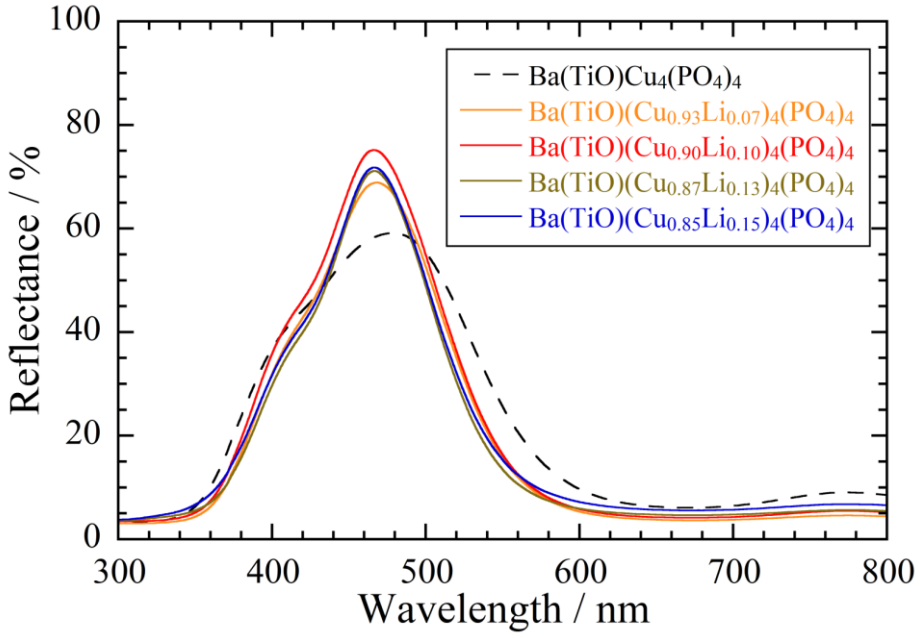

Fig. 1.5 UV-vis diffuse reflectance spectra of the $Ba(TiO)(Cu_{1-x}Li_x)_4(PO_4)_4$ samples.

of blue) decreased with increasing Li concentration (x), while the reflectance from 435 to 480 nm (blue) increased with increasing x. In general, when square planar CuO_4 units exist in the structure, the *d*–*d* transition of Cu^{2+} consists of three broad transitions that correspond to $^2B_{1g} \rightarrow {}^2B_{2g}$, $^2B_{1g} \rightarrow {}^2E_g$, and $^2B_{1g} \rightarrow {}^2A_{1g}$ in the order from the long-wavelength side, and only the $^2B_{1g} \rightarrow {}^2B_{2g}$ transition appears outside of visible light region among three [36]. The distortion of CuO_4 unit to a tetrahedral configuration from square planar shape causes the splitting of the *d* orbitals to decrease, as shown in Fig. 1.6. As a result, the *d*–*d* transition in visible light region which is mainly composed of $^2B_{1g} \rightarrow {}^2E_g$ (d_{yz}, $d_{zx} \rightarrow d_{x2-y2}$), and $^2B_{1g} \rightarrow {}^2A_{1g}$ ($d_{z2} \rightarrow d_{x2-y2}$) were shifted to longer wavelength and its transition probability increased. Moreover, increase of the lattice size elongates the distance between Cu and O, resulting in the shift of the charge transfer absorption toward shorter wavelength. As a result of the absorption shift of *d*–*d* transition and charge transfer, the overlap of them in the wavelength region of 435 to 480 nm was thus reduced, resulting in an increase of the reflectance in this region. In addition, I consider that the decrease in the reflectance in the 580 to 595 nm wavelength region was caused by an increase in *d*–*d* transition absorption due to the increase of *d*–*d* transition probability arising from the distortion. On the other hand, for the samples with $x > 0.10$,

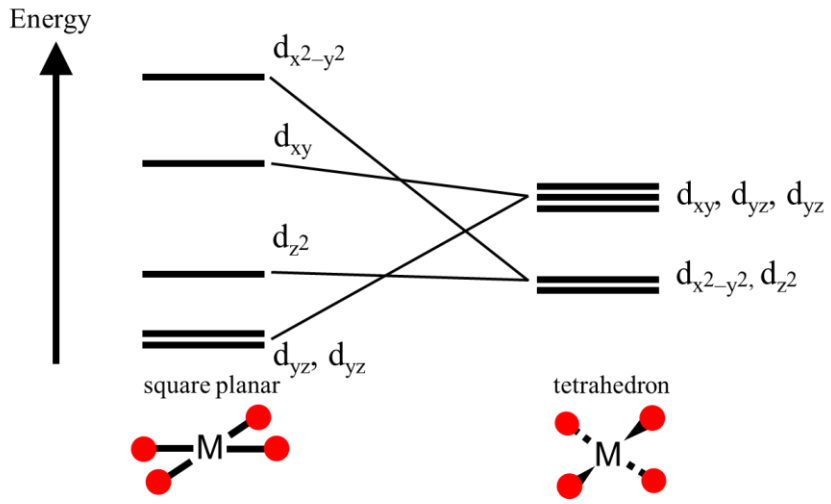

Fig. 1.6 *d* orbital splitting for square planar and tetrahedron MO_4 units.

reflectance in the wavelength regions below 370 nm and above 580 nm increased and reflectance between 435 and 480 nm decreased, compared to that of the sample with $x = 0.10$. This is due to the increase of reflectance in the entire visible light region by the reflection of the white TiO_2 impurity as well as the absorption in the wavelength region between 435 and 480 nm by $Cu_2P_2O_7$. Table 1.2 lists the color parameters of the $Ba(TiO)(Cu_{1-x}Li_x)_4(PO_4)_4$ ($0 \leq x \leq 0.15$) samples, and the photographs of the samples with $x = 0$ and 0.10 are displayed in Fig. 1.7. Although the $Ba(TiO)Cu_4(PO_4)_4$ mother solid showed a light blue color with a blueness value ($-b^*$) of 38.2, the $-b^*$ value was increased monotonically with increasing Li^+ content up to $x = 0.10$, and the highest blueness value ($b^* = -57.6$) was obtained for the $Ba(TiO)(Cu_{0.90}Li_{0.10})_4(PO_4)_4$ solid to exhibit a vivid blue color. On the other hand, the blueness values of the samples including impurity phases were lower than that of the $Ba(TiO)(Cu_{0.90}Li_{0.10})_4(PO_4)_4$ solid. This tendency was consistent with the UV-vis diffuse reflectance spectra. Compared to the two commercially available blue pigments, the blueness value ($-b^*$) of the $Ba(TiO)(Cu_{0.90}Li_{0.10})_4(PO_4)_4$ sample was higher than that of $Fe^{III}_4[Fe^{II}(CN)_6]_3$ (dark blue; $b^* = -19.3$) and almost the same as that of $CoAl_2O_4$ (cobalt blue; $b^* = -59.5$), while the brightness value (L^*) is high, as listed in Table 1.3. However, since the hue angle ($H° = 268.7$) of the prepared $Ba(TiO)(Cu_{0.90}Li_{0.10})_4(PO_4)_4$ solid is very close to 270°, it is found that the $Ba(TiO)(Cu_{0.90}Li_{0.10})_4(PO_4)_4$ solid shows a vivid light blue color compared with the commercially

available blue pigments (Fig. 1.8).

Table 1.2 Color parameters of the $Ba(TiO)(Cu_{1-x}Li_x)_4(PO_4)_4$ ($0 \leq x \leq 0.15$) samples

Sample	*L**	*a**	*b**	*C*	*H*°
$Ba(TiO)Cu_4(PO_4)_4$	59.0	−18.5	−38.2	42.5	244.1
$Ba(TiO)(Cu_{0.93}Li_{0.07})_4(PO_4)_4$	52.9	−5.5	−54.7	55.0	264.2
$Ba(TiO)(Cu_{0.90}Li_{0.10})_4(PO_4)_4$	52.2	−1.4	−57.6	57.6	268.7
$Ba(TiO)(Cu_{0.87}Li_{0.13})_4(PO_4)_4$*	52.1	−1.0	−55.2	55.2	269.0
$Ba(TiO)(Cu_{0.85}Li_{0.15})_4(PO_4)_4$*	53.2	−1.0	−53.9	53.9	269.0

* Mixed phase sample

Fig. 1.7 Photographs of the (a) $Ba(TiO)Cu_4(PO_4)_4$ and (b) $Ba(TiO)(Cu_{0.90}Li_{0.10})_4(PO_4)_4$ samples.

Table 1.3 Color parameters of the $Ba(TiO)(Cu_{0.90}Li_{0.10})_4(PO_4)_4$, $Fe^{III}_4[Fe^{II}(CN)_6]_3$ (navy blue), and $CoAl_2O_4$ (cobalt blue)

Sample	*L**	*a**	*b**	*C*	*H*°
$Ba(TiO)(Cu_{0.90}Li_{0.10})_4(PO_4)_4$	52.2	−1.4	−57.6	57.6	268.7
$Fe^{III}_4[Fe^{II}(CN)_6]_3$	4.0	15.0	−19.3	24.4	307.9
$CoAl_2O_4$	37.8	21.6	−59.5	63.3	290.9

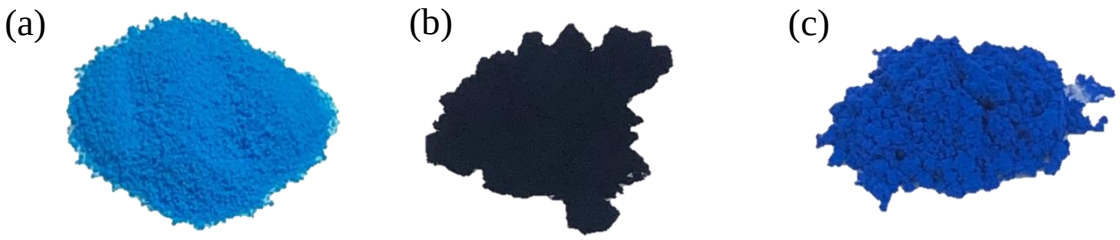

Fig. 1.8 Photographs of (a) $Ba(TiO)(Cu_{0.90}Li_{0.10})_4(PO_4)_4$, (b) $Fe^{III}_4[Fe^{II}(CN)_6]_3$ (navy blue), and (c) $CoAl_2O_4$ (cobalt blue).

Acid, thermal, and light-resistance tests were carried out to evaluate the durability of the $Ba(TiO)(Cu_{0.90}Li_{0.10})_4(PO_4)_4$ pigment and the color difference (ΔE^*_{ab}) of the sample was calculated from the following equation (1-1).

$$\Delta E^*_{ab} = [(\Delta L^*)^2 + (\Delta a^*)^2 + (\Delta b^*)^2]^{1/2} \quad (1\text{-}1)$$

A small ΔE^*_{ab} means high durability of the pigment. As shown in Table 1.4, no significant color change was confirmed even by heating and irradiating UV light, indicating that the $Ba(TiO)(Cu_{0.90}Li_{0.10})_4(PO_4)_4$ pigment has high resistance against both heat and UV irradiation. However, ΔE^*_{ab} value (8.41) for acid treatment is relatively large, confirming that the acid resistance of this pigment is insufficient.

Table 1.4 Color parameters of the $Ba(TiO)(Cu_{0.90}Li_{0.10})_4(PO_4)_4$ after acid, thermal, and light resistance test

Sample	L^*	a^*	b^*	ΔE_{ab}^*
Before treatment	52.2	−1.4	−57.6	-
After acid treatment	58.1	−9.4	−51.8	8.41
After thermal treatment	51.9	−0.3	−56.2	1.81
After UV irradiation	49.6	−1.4	−57.3	2.62

1.4 Conclusion

In conclusion, novel environmentally friendly inorganic blue pigments that do not contain toxic elements such as Co^{2+}, $Ba(TiO)(Cu_{1-x}Li_x)_4(PO_4)_4$ ($0 \le x \le 0.15$), were prepared by a solid-state reaction method. To obtain a vivid blue color, the absorption bands due to the charge transfer from O^{2-} to Cu^{2+} and the *d–d* transition of Cu^{2+} of the $Ba(TiO)Cu_4(PO_4)_4$ solid were intentionally controlled by introducing Li^+ with a larger ionic radius and lower valence than Cu^{2+} to distort the square planar CuO_4 units. The most vivid blue color was obtained for the $Ba(TiO)(Cu_{0.90}Li_{0.10})_4(PO_4)_4$ solid with the $L^*a^*b^*CH°$ color parameters of $L^* = 52.2$, $a^* = -1.4$, $b^* = -57.6$, $C = 57.6$, and $H° = 268.7$. The blueness parameter $-b^*$ was almost equal to that of toxic

$CoAl_2O_4$ (cobalt blue) and the hue angle $H°$ was closer to pure blue compared with $CoAl_2O_4$. Since the $Ba(TiO)(Cu_{0.90}Li_{0.10})_4(PO_4)_4$ pigment possesses the high thermal and UV irradiation durability, it is expected to be a candidate for novel environmentally friendly inorganic blue pigments.

Chapter 2

Novel Environmentally Friendly Inorganic Blue Pigments Based on $Li_2Cu_5(PO_4)_4$

2.1 Introduction

In chapter 1, it was found that distortion of the CuO_4 unit in the $Ba(TiO)Cu_4(PO_4)_4$ by the partial substitution of Li^+ for Cu^{2+} caused a shift of absorption wavelength derived from Cu^{2+} to give a vivid blue color. However, the resistance for acid of the Li^+ doped $Ba(TiO)Cu_4(PO_4)_4$ is insufficient, which should restrict the practical application use.

Therefore, in this chapter, I aim to develop a new blue inorganic pigment having high blueness value and high durability. Here, I select $Li_2Cu_5(PO_4)_4$ which has the square planar CuO_4 unit in the structure [42] similar to the $Ba(TiO)Cu_4(PO_4)_4$. Although the $Li_2Cu_5(PO_4)_4$ solid has been reported to exhibit greenish blue color [42], it is expected to improve the blueness of $Li_2Cu_5(PO_4)_4$ solid by controlling the $d-d$ transition absorption, similar to the case for $Ba(TiO)Cu_4(PO_4)_4$. For the distortion of CuO_4 unit in the $Li_2Cu_5(PO_4)_4$ solid, Na^+ ions (0.099 nm, CN = 4) [40] are doped into the Li^+ ion (0.059 nm, CN = 4) [40] site, which induces indirectly a distortion of CuO_4 unit via Li–O–Cu bonding. Such indirect distortion of CuO_4 unit does not lower the Cu^{2+} content in the $Li_2Cu_5(PO_4)_4$ solid, which is also effective for obtaining high blueness value.

2.2 Experimental procedure

The $(Li_{1-x}Na_x)_2Cu_5(PO_4)_4$ ($0 \leq x \leq 0.20$) solids were synthesized using a conventional solid-state reaction method. After premixing of starting materials of Li_2CO_3, Na_2CO_3, CuO, and $(NH_4)_2HPO_4$ with an agate mortar, the mixed powder was mechanically mixed using a planetary ball mill (P-7, FRITSCH GmbH) at 300 rpm for 1 h in atmospheric air. For all samples, 110% of the

stoichiometric amounts of Li_2CO_3 and Na_2CO_3 and 105% of $(NH_4)_2HPO_4$ were mixed to suppress the generation of the impurity phases such as $Li_2Cu_4P_2O_{10}$ and $Cu_4O(PO_4)_2$. The mixed powders were heated at 600 °C for 10 h in air. After grinding the obtained powders by an agate mortar, the sample powders were calcined at 850 °C for 24 h in air.

X-ray powder diffraction measurements (XRD; SmartLab, Rigaku Co.) with Cu Kα radiation (40 kV, 30 mA) were conducted to confirm the crystal structure and the generation of impurity phase. The optical properties were investigated by recording diffuse reflectance spectra using UV-visible spectrophotometry (UV-2600, Shimadzu Co.) with barium sulfate as a reference. The color properties of the samples were investigated in terms of the CIE *L*a*b** system using a colorimetry (CR-400, Konica Minolta, Inc.).

As same as the chapter 1, acid resistance was tested by dispersing the sample powder in a 4 wt% acetic acid aqueous solution. After stirring for 30 min, the sample was filtered, washed with deionized water and ethanol, and dried at room temperature. The thermal resistance test was performed by heating the sample at 850 °C for 24 h in air. The light resistance test was carried out by irradiating the sample with a UV lamp (EFD15BLB, Toshiba Co.) with an emission wavelength of 352 nm for 100 h. The color differences of the pigments after each resistance test were evaluated using color parameters.

2.3 Results and discussion

Figure 2.1 shows the XRD patterns of the $(Li_{1-x}Na_x)_2Cu_5(PO_4)_4$ ($0 \leq x \leq 0.20$) samples. All samples were found to hold the single-phase of $Li_2Cu_5(PO_4)_4$ structure without any additional impurities. The lattice volumes calculated from the XRD peak angles are shown in Fig. 2.2. The lattice volume increases with increasing Na^+ content (x) up to 0.10 because of the larger ionic radius of Na^+ (0.099 nm, CN = 4) [40] than that of Li^+ (0.059 nm, CN = 4) [40]. On the other hand, the solids with $x > 0.10$ have the similar lattice volume of the sample with $x = 0.10$ while much amount

of Na^+ doped into the $Li_2Cu_5(PO_4)_4$ solid. This phenomenon suggests an excess amount of Na^+ probably forms an amorphous material in the grain boundary, which is quite difficult to confirm by XRD measurements, for the samples with Na^+ content higher than 0.10. Therefore, the samples with $x \leq 0.10$ can form a single-phase of solid solution in which Na^+ ions partially substitute for Li^+ site in the $(Li_{1-x}Na_x)_2Cu_5(PO_4)_4$ solids.

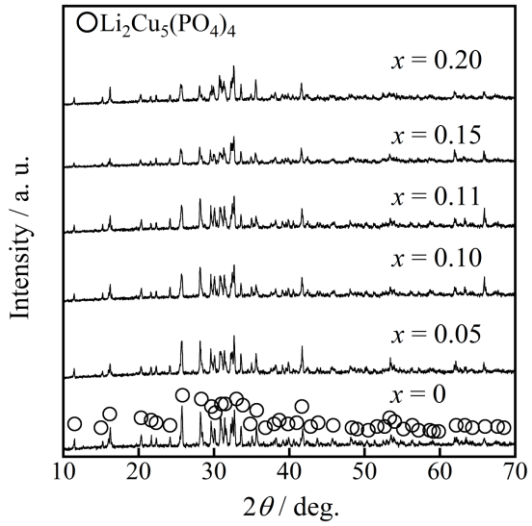

Fig. 2.1 XRD patterns of the $(Li_{1-x}Na_x)_2Cu_5(PO_4)_4$ samples.

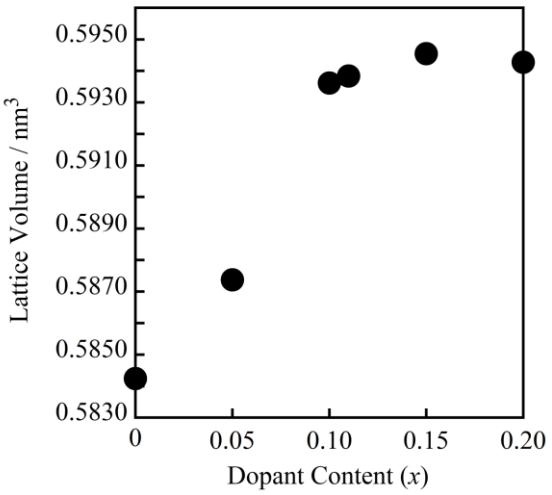

Fig. 2.2 Lattice volumes of the $(Li_{1-x}Na_x)_2Cu_5(PO_4)_4$ samples.

Figure 2.3 depicts the UV-vis diffuse reflectance spectra of the $(Li_{1-x}Na_x)_2Cu_5(PO_4)_4$ ($0 \leq x \leq 0.20$) without the spectrum for the solid with $x = 0.11$ because of the quite similar spectra to the solid with $x = 0.10$, whose deference is difficult to confirm by this figure. All samples exhibited strong optical absorption at wavelengths shorter and longer than 480 nm, resulting in the strong reflection with the peak top at 480 nm. These two optical absorptions are attributed to the charge transfer transition from O^{2-} to Cu^{2+} at wavelengths shorter than 480 nm and the *d–d* transition of Cu^{2+} [24] at wavelengths longer than 480 nm. For the samples with $x \leq 0.10$, the reflectance in the green region at wavelengths between 520 and 560 nm decreases with increasing Na^+ concentration (x) (Fig. 2.3 (b)). If the absorption at this wavelength region is increased simply by the shift of *d–d*

transition absorption toward shorter wavelength, the reflectance around 490 nm may also decrease. However, the reflectance at this region oppositely increased, meaning that *d–d* transition absorption shifts to the longer wavelength.

Because of the increase of lattice volume for the solids with $x \leq 0.1$ (Fig. 2.2), Cu–O distance in the structure may be elongated, suggesting the reduction of the *d* orbital splitting of Cu caused by the weakening of the crystal field of Cu. Therefore, the *d–d* transition absorption of $^2B_{1g} \rightarrow {}^2A_{1g}$ which appears in the shortest wavelength region (centered around 540 nm [36]) of the three kinds of *d–d* transition should be strengthened and shifted toward longer wavelengths by the substitution of larger Na^+ ions into Li^+ sites. As a result of such change in *d–d* transition absorption, absorbance of the green region is increased and the samples with $x = 0.05$ and 0.10 showed higher blueness value ($-b^*$) and lower greenness value ($-a^*$) than those of the sample with $x = 0$ (Table 2.1). For the sample with $x = 0.15$ obtained as a mixed-phase, a similar trend in *d–d* transition absorption of $^2B_{1g} \rightarrow {}^2A_{1g}$ was observed for the sample with $x = 0.10$. However, the reflectance in the yellow region at wavelengths between 580 and 595 nm was increased compared with the sample with $x = 0.10$ likely due to the reflection of the amorphous impurity phase. As a result of increase in reflectance at the yellow region which is the complementary color of blue, blueness ($-b^*$) decreased. Moreover, for the sample with $x = 0.20$ which may contain a larger amount of amorphous impurity phase than the sample with $x = 0.15$, the reflectance in the entire visible light region was increased. From these results, it was found that $(Li_{0.90}Na_{0.10})_2Cu_5(PO_4)_4$ has a high blueness value ($b^* = -39.4$) and a hue angle ($H^\circ = 246.0^\circ$). Figure 2.4 presents a photograph of the $(Li_{0.90}Na_{0.10})_2Cu_5(PO_4)_4$ sample powder and the nontoxic commercial $Fe^{III}{}_4[Fe^{II}(CN)_6]_3$. It is obvious that the $(Li_{0.90}Na_{0.10})_2Cu_5(PO_4)_4$ sample has a vivid blue color.

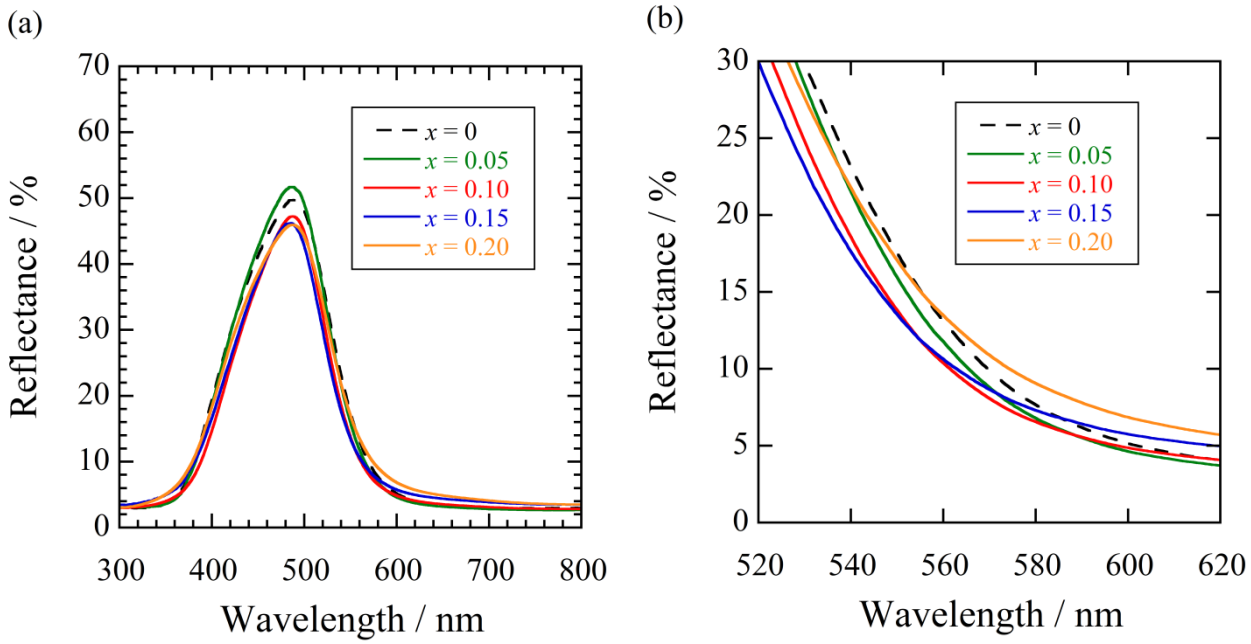

Fig. 2.3 (a) UV-vis diffuse reflectance spectra and (b) its magnified view in the range from 520 to 620 nm for the $(Li_{1-x}Na_x)_2Cu_5(PO_4)_4$ ($0 \leq x \leq 0.20$) samples.

Table 2.1 Color parameters of $(Li_{1-x}Na_x)_2Cu_5(PO_4)_4$ ($0 \leq x \leq 0.20$) and $Fe^{III}_4[Fe^{II}(CN)_6]_3$ (navy blue)

Samples	*L**	*a**	*b**	*C*	*H*°
$Li_2Cu_5(PO_4)_4$	54.4	−25.3	−38.3	45.9	236.6
$(Li_{0.95}Na_{0.05})_2Cu_5(PO_4)_4$	52.5	−22.7	−39.8	45.8	240.3
$(Li_{0.90}Na_{0.10})_2Cu_5(PO_4)_4$	48.9	−17.6	−39.4	43.1	246.0
$(Li_{0.89}Na_{0.11})_2Cu_5(PO_4)_4$	49.0	−17.0	−38.2	41.8	246.0
$(Li_{0.85}Na_{0.15})_2Cu_5(PO_4)_4$	49.3	−15.4	−37.0	40.1	247.4
$(Li_{0.80}Na_{0.20})_2Cu_5(PO_4)_4$	53.6	−18.5	−34.1	38.8	241.5
Commercial $Fe^{III}_4[Fe^{II}(CN)_6]_3$	4.0	15.0	−19.3	24.4	307.9

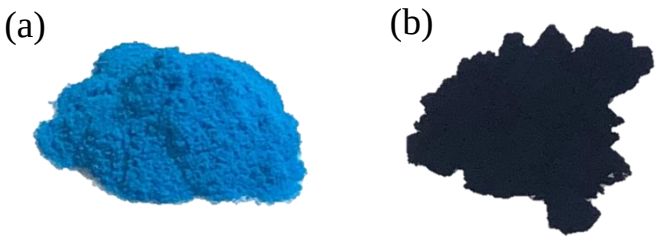

Fig. 2.4 Photographs of (a) $(Li_{0.90}Na_{0.10})_2Cu_5(PO_4)_4$ and (b) $Fe^{III}_4[Fe^{II}(CN)_6]_3$ (navy blue).

Acid, thermal, and light resistances of the $(Li_{0.90}Na_{0.10})_2Cu_5(PO_4)_4$ pigment were evaluated with the color differences (ΔE^*_{ab}). As listed in Table 2.2, the ΔE^*_{ab} values for the $(Li_{0.90}Na_{0.10})_2Cu_5(PO_4)_4$ solid upon acid treatment, heating, and UV irradiation is 1.57, 1.18, and 1.48 respectively, which were enough small value in general. In addition, since the values are smaller than those for $Ba(TiO)(Cu_{0.90}Li_{0.10})_4(PO_4)_4$ pigment in the chapter 1, it was found that the $(Li_{0.90}Na_{0.10})_2Cu_5(PO_4)_4$ pigment is highly durable against acid, heat, and UV irradiation.

Table 2.2 Color parameters of the $(Li_{0.90}Na_{0.10})_2Cu_5(PO_4)$ after acid, thermal, and light resistance test

Sample	L^*	a^*	b^*	ΔE_{ab}^*
Before treatment	48.9	−17.6	−39.4	-
After acid treatment	47.4	−17.2	−39.6	1.57
After thermal treatment	47.9	−17.6	−39.2	1.18
After UV irradiation	47.6	−17.1	−38.9	1.48

2.4 Conclusion

To develop a novel environmentally friendly inorganic blue pigments having high resistance against acid, heat, and UV irradiation, $(Li_{1-x}Na_x)_2Cu_5(PO_4)_4$ ($0 \leq x \leq 0.20$) were synthesized by a conventional solid-state reaction method. To obtain a vivid blue color by reducing the absorption at green light region, the *d*–*d* transition absorption of $Li_2Cu_5(PO_4)_4$ was controlled by the introduction of larger Na^+ into the Li^+ site. As a result, a vivid blue color with the blueness value of $b^*= -39.4$ was successfully obtained. In addition, the $(Li_{0.90}Na_{0.10})_2Cu_5(PO_4)_4$ pigment possesses high acid, thermal, and UV irradiation durability.

Chapter 3

Novel Environmentally Friendly Inorganic Blue Pigments Based on $Na_4Cu(PO_4)_2$

3.1 Introduction

In chapters 1 and 2, I demonstrated that the compounds having square planar CuO_4 units in the structure are the candidates for environmentally friendly inorganic blue pigment and intentional distortion of CuO_4 unit is an effective strategy for improving the blue hue. However, the number of candidate structure which contains a square planar CuO_4 unit are limited, and therefore, it should be expanded to search the candidate materials for other materials in which the CuO_x unit existed in its structure.

In this chapter, $Na_4Cu(PO_4)_2$ was selected as a mother solid, which is composed of nontoxic elements including Cu^{2+} while the crystal structure has not been clarified yet [43]. Because the absorbed wavelength of visible light is influenced by the coordination environment of color source ions as mentioned in the previous chapters, the color hue of $Na_4Cu(PO_4)_2$ by distorting the CuO_x units (Cu–O bond length and O–Cu–O angle) can be also controlled. Because both the Cu–O bond length and O–Cu–O angle are influenced by the cation size of Cu site and bond strength between Cu site and surrounding O, they can be tuned by doping cations having different electronegativity as well as the aliovalent valence state (chapter 1) and/or different ionic size (chapter 2). Therefore, here, the Cu^{2+} (radius: 0.057 nm (CN = 4) [40], electronegativity (χ): 1.90 [44]) site of the $Na_4Cu(PO_4)_2$ was partially replaced with various divalent cations, Mg^{2+} (0.057 nm (CN = 4) [40], χ = 1.31 [44]), Ca^{2+} (0.100 nm (CN = 6) [40], χ = 1.00 [44]), and Zn^{2+} (0.060 nm (CN = 4) [40], χ = 1.65 [44]), and the color properties of the $Na_4Cu_{1-x}M_x(PO_4)_2$ (M = Mg^{2+}, Ca^{2+}, Zn^{2+}) were investigated.

3.2 Experimental procedure

$Na_4Cu_{1-x}M_x(PO_4)_2$ (M = Mg^{2+}, Ca^{2+}, Zn^{2+}) solids were synthesized by a conventional solid-state reaction with Na_2HPO_4, CuO, and $MgCO_3$, $CaCO_3$, and ZnO as the starting materials. After mixing the starting materials using an agate mortar, the mixed powder was calcined at 850 °C for 12 h in synthetic air.

The samples were identified by X-ray powder diffraction (XRD; SmartLab, Rigaku) with Cu Kα radiation (40 kV, 30 mA). The optical reflectance spectra were recorded using UV-visible spectrophotometry (UV-2600, Shimadzu) with barium sulfate as a reference. The color properties of the samples were investigated in terms of the CIE *L*a*b** system using a colorimetry (CR-400, Konica-Minolta). As same as the chapters 1 and 2, acid, thermal, and light (UV) resistances were investigated.

3.3 Results and discussion

Figure 3.1 depicts the XRD patterns of the $Na_4Cu(PO_4)_2$ and $Na_4Cu_{0.90}M_{0.10}(PO_4)_2$ (M = Mg^{2+}, Ca^{2+}, Zn^{2+}) solids. The samples doped with Mg^{2+} (0.057 nm, CN = 4) [40] and Zn^{2+} (0.060 nm, CN = 4) [40] having close ionic radius to Cu^{2+} (0.057 nm, CN = 4) [40] showed the same diffraction pattern as the mother $Na_4Cu(PO_4)_2$ solid. In addition, a slight peak shift toward lower angle was observed for the $Na_4Cu_{0.90}Zn_{0.10}(PO_4)_2$ compared with mother $Na_4Cu(PO_4)_2$ solid, while an apparent peak shift was not confirmed for the $Na_4Cu_{0.90}Mg_{0.10}(PO_4)_2$ because of the same ionic radii of $Mg^{2+}$and Cu^{2+}. For the solid with M = Ca^{2+} whose ionic size (0.100 nm, CN = 6) [40] is large compared with Cu^{2+}, the sample was obtained as the two-phase mixture of $Na_4Cu(PO_4)_2$ and $Ca_2P_2O_7$. From these results, it was confirmed that the $Na_4Cu_{0.90}M_{0.10}(PO_4)_2$ (M = Mg^{2+}, Zn^{2+}) solids form a solid solution.

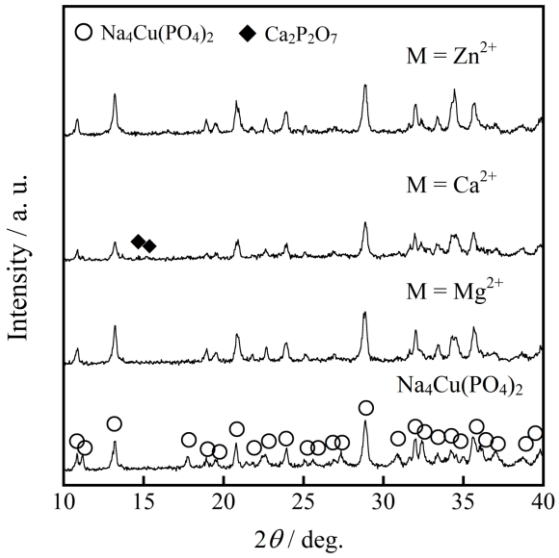

Fig. 3.1 XRD patterns of the $Na_4Cu(PO_4)_2$ and the $Na_4Cu_{0.90}M_{0.10}(PO_4)_2$ ($M = Mg^{2+}$, Ca^{2+}, Zn^{2+}) solids.

Figure 3.2 and Table 3.1 present the UV-vis diffuse reflectance spectra and the color parameters of the $Na_4Cu_{0.90}M_{0.10}(PO_4)_2$ ($M = Mg^{2+}$, Zn^{2+}) solids obtained as single-phase sample, respectively, with those for mother $Na_4Cu(PO_4)_2$ solid. Both the $Na_4Cu_{0.90}M_{0.10}(PO_4)_2$ ($M = Mg^{2+}$, Zn^{2+}) solids absorb light at wavelengths shorter and longer than ca. 460 nm as same as the $Na_4Cu(PO_4)_2$ solid, which is mainly due to the charge transfer transition from O^{2-} to Cu^{2+} and the *d*–*d* transition of Cu^{2+}, respectively [24]. As a result of absorption at these wavelengths, all the solids showed a single reflectance spectrum with a peak top of ca. 460 nm (blue to green color) in the visible light region. For the $Na_4Cu_{0.90}Mg_{0.10}(PO_4)_2$ solid, the absorption by the charge transfer transition from O^{2-} to Cu^{2+} is decreased and that by the *d*–*d* transition of Cu^{2+} is increased. This behavior can be explained from the viewpoint of local displacement around Cu^{2+} in the structure. By the partial substitution of Mg^{2+} whose electronegativity ($\chi = 1.31$) [44] is smaller than the Cu^{2+} ($\chi = 1.90$) [44], a slight displacement of ions surrounding Cu^{2+} raises the partial elongation of Cu–O bonding, which causes the decrease of charge transfer from O^{2-} to Cu^{2+}. Furthermore, the distortion of the Cu–O unit may increase a probability of *d*–*d* transition whose forbidden state may be partially

allowed by lowering the degree of symmetry around Cu^{2+}. On the other hand, the $Na_4Cu_{0.90}Zn_{0.10}(PO_4)_2$ solid showed lower reflectance entirely in the visible light region compared with the mother $Na_4Cu(PO_4)_2$ solid. This is due to the electronic state of Zn^{2+}. Similar to the case for Mg^{2+}, doping of Zn^{2+} having larger ionic size and slightly smaller electronegativity (χ = 1.65) [44] compared with Cu^{2+} will cause the elongation of Cu–O bonding together with the lowering of the symmetry around Cu^{2+}. Therefore, the absorption by *d*–*d* transition is increased. However, on the contrary of the case for Mg^{2+} doping, charge transfer transition at shorter wavelengths also increases, which can be explained by the partial participation of *d* orbitals of Zn^{2+} located at an energy level close to the O 2p orbital to the charge transfer transition from O^{2-} to Cu^{2+}. As a result, the solid doped with Zn^{2+} showed lower reflectance at blue region compared with the mother $Na_4Cu(PO_4)_2$ solid. From these results, it is obvious that the $Na_4Cu_{0.90}Mg_{0.10}(PO_4)_2$ solid possesses the higher blueness value (b^* = −36.1) than that (b^* = −26.4) of the mother $Na_4Cu(PO_4)_2$ solid and the hue angle ($H°$ = 257.8°) close to the pure blue hue angle ($H°$ = 270°).

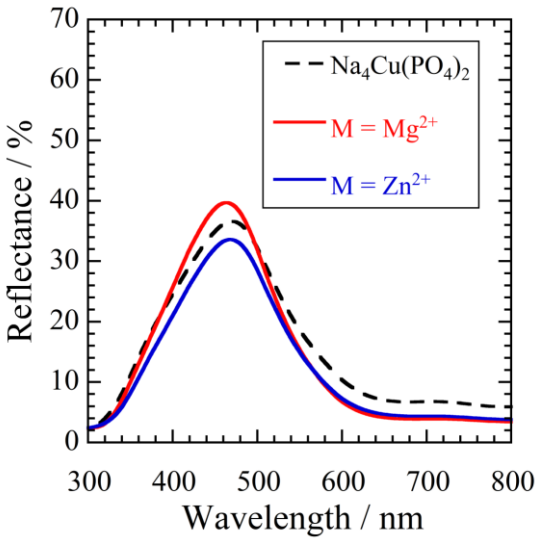

Fig. 3.2 UV-vis diffuse reflectance spectra of the $Na_4Cu(PO_4)_2$ and the $Na_4Cu_{0.90}M_{0.10}(PO_4)_2$ (M = Mg^{2+}, Ca^{2+}, Zn^{2+}) solids.

Table 3.1 Color parameters of $Na_4Cu(PO_4)_2$ and $Na_4Cu_{0.90}M_{0.10}(PO_4)_2$ ($M = Mg^{2+}$, Zn^{2+})

Samples	*L**	*a**	*b**	*C*	*H*°
$Na_4Cu(PO_4)_2$	52.1	−10.9	−26.4	28.6	247.6
$Na_4Cu_{0.90}Mg_{0.10}(PO_4)_2$	47.6	−7.8	−36.1	36.9	257.8
$Na_4Cu_{0.90}Zn_{0.10}(PO_4)_2$	46.8	−9.4	−31.8	33.2	253.6

To improve the blueness of the Mg^{2+} doped $Na_4Cu(PO_4)_2$ solid, the composition of the $Na_4Cu_{1-x}Mg_x(PO_4)_2$ solid was optimized. Figure 3.3 shows the XRD patterns of the $Na_4Cu_{1-x}Mg_x(PO_4)_2$ ($0 \leq x \leq 0.25$). For the samples with $x \leq 0.20$, only peaks corresponding to the $Na_4Cu(PO_4)_2$ phase were observed. However, an additional peak assigned to the $Cu_2P_2O_7$ phase was also confirmed for the samples with $x = 0.25$, while the ionic radii of Mg^{2+} and Cu^{2+} are the same. This is probably due to much amount of Mg^{2+} with low electronegativity causes so large distortion that the sample cannot maintain the $Na_4Cu(PO_4)_2$ type structure.

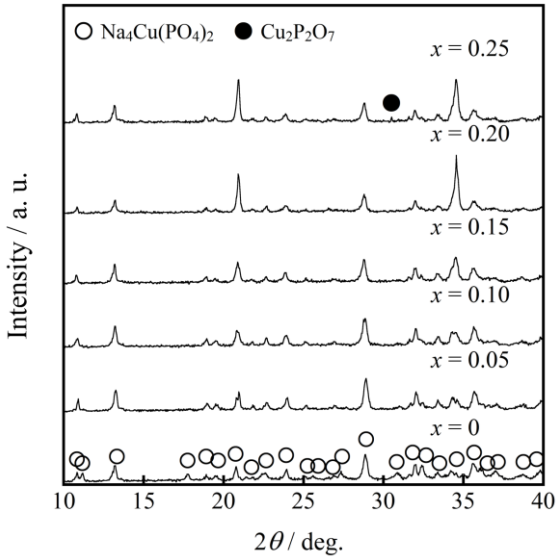

Fig. 3.3 XRD patterns of the $Na_4Cu_{1-x}Mg_x(PO_4)_2$ ($0 \leq x \leq 0.25$) solids.

Figure 3.4 displays the UV-vis diffuse reflectance spectra of $Na_4Cu_{1-x}Mg_x(PO_4)_2$ ($0 \leq x \leq 0.20$) holding the single phase of the $Na_4Cu(PO_4)_2$ structure and their color parameters are listed in Table 3.2. For the samples with $x \leq 0.15$, the reflectance at blue region around 460 nm and blueness value ($-b^*$) were increased with increasing Mg^{2+} content x. This is by the effect of the Mg^{2+} doping as explained above. For the sample with $x = 0.20$, the reflectance around 460 nm is lower than the sample with $x = 0.15$ while the change in optical absorption possibly occurred similar to the samples with $x \leq 0.15$. This is due to the absorption of the impurity $Cu_2P_2O_7$ phase which was not observed evidently in the XRD pattern but might be contaminated in the solid for the sample with $x = 0.20$. From these results, $Na_4Cu_{0.85}Mg_{0.15}(PO_4)_2$ with the highest reflectance around the blue region in the UV-vis diffuse reflectance spectra has the highest blueness value ($-b^*$) of 38.2. Figure 3.5 presents a photograph of the $Na_4Cu_{0.85}Mg_{0.15}(PO_4)_2$ sample powder with the nontoxic commercial $Fe^{III}_4[Fe^{II}(CN)_6]_3$ (navy blue). The $Na_4Cu_{0.85}Mg_{0.15}(PO_4)_2$ sample was found to have higher chroma parameter (C) and hue angle ($H°$) with high brightness value (L^*), indicating the vivid blue color was obtained.

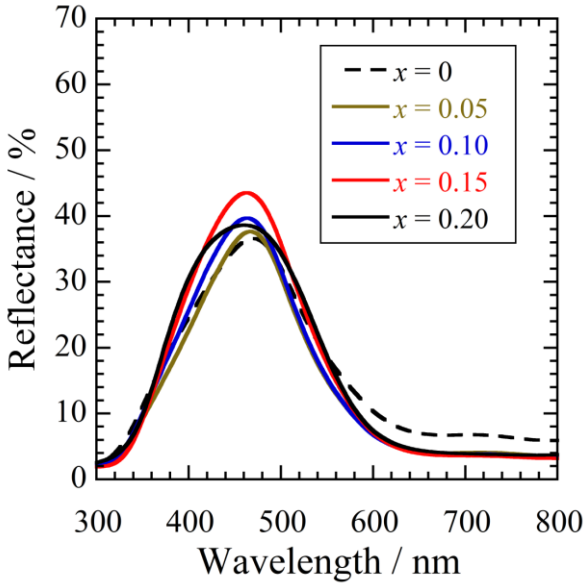

Fig. 3.4 UV-vis diffuse reflectance spectra of the $Na_4Cu_{1-x}Mg_x(PO_4)_2$ ($0 \leq x \leq 0.20$) solids.

Table 3.2 Color parameters of $Na_4Cu_{1-x}Mg_x(PO_4)_2$ ($0 \leq x \leq 0.20$) and $Fe^{III}_4[Fe^{II}(CN)_6]_3$ (navy blue)

Samples	*L**	*a**	*b**	*C*	*H*°
$Na_4Cu(PO_4)_2$	52.1	−10.9	−26.4	28.6	247.6
$Na_4Cu_{0.95}Mg_{0.05}(PO_4)_2$	46.6	−8.6	−33.8	34.9	255.7
$Na_4Cu_{0.90}Mg_{0.10}(PO_4)_2$	47.6	−7.8	−36.1	36.9	257.8
$Na_4Cu_{0.85}Mg_{0.15}(PO_4)_2$	49.9	−9.3	−38.2	39.3	256.4
$Na_4Cu_{0.80}Mg_{0.20}(PO_4)_2$	48.7	−13.4	−36.4	38.7	249.8
Commercial $Fe^{III}_4[Fe^{II}(CN)_6]_3$	4.0	15.0	−19.3	24.4	307.9

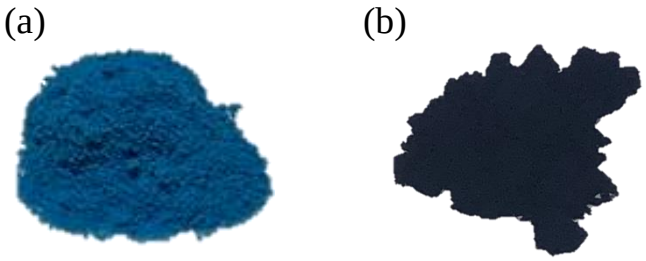

Fig. 3.5 Photographs of (a) $Na_4Cu_{0.85}Mg_{0.15}(PO_4)_2$ and (b) $Fe^{III}_4[Fe^{II}(CN)_6]$ (navy blue).

Table 3.3 lists the color differences (ΔE^*_{ab}) values for acid and heat treatment and UV irradiation for the $Na_4Cu_{0.85}Mg_{0.15}(PO_4)_2$ pigment. Although the sample after acid treatment was not able to be recovered due to its dissolution, the $Na_4Cu_{0.85}Mg_{0.15}(PO_4)_2$ pigment has small ΔE^*_{ab} value (2.02) for heat treatment together with that (1.52) for UV irradiation, indicating that the $Na_4Cu_{0.85}Mg_{0.15}(PO_4)_2$ pigment is highly durable against both heat and UV irradiation.

Table 3.3 Color parameters of the $Na_4Cu_{0.85}Mg_{0.15}(PO_4)_2$ after acid, thermal, and light resistance test

Sample	*L**	*a**	*b**	ΔE_{ab}*
Before treatment	49.9	−9.3	−38.2	-
After acid treatment	-	-	-	-
After thermal treatment	47.9	−9.3	−38.5	2.02
After UV irradiation	48.6	−9.9	−37.7	1.52

3.4 Conclusion

To evaluate the effect of electronegativity of dopants on the coordination environment around Cu^{2+}, various divalent ions were doped into Cu^{2+} site in $Na_4Cu(PO_4)_2$ for the intentional control of charge transfer and the *d*–*d* transition absorptions of the $Na_4Cu(PO_4)_2$ solid. Since the $Na_4Cu_{0.85}Mg_{0.15}(PO_4)_2$ in which Mg^{2+} with lower electronegativity than Cu^{2+} doped into the Cu^{2+} site showed a highest blueness value ($-b^*$) of 38.2 because of elongation of Cu–O distance, it was revealed that the strategy which distortion of CuO_x unit is realized by tuning the electronegativity of Cu^{2+} site is also effective for improving blue hue of the materials containing Cu^{2+} as a color source.

Summary

In the study of this thesis, novel environmentally friendly inorganic blue pigments with Cu^{2+} as a color source have been successfully obtained and their color properties were investigated. Moreover, the strategy for improving the blue color hue of the pigments whose color source is Cu^{2+} has been proposed.

The results and findings obtained through this study are summarized as follows:

Chapter 1

Novel environmentally friendly inorganic blue pigments, $Ba(TiO)(Cu_{1-x}Li_x)_4(PO_4)_4$ solids were successfully synthesized by a conventional solid-state reaction method. By partial substitution of the Cu^{2+} site in the $Ba(TiO)Cu_4(PO_4)_4$ solid with Li^+, the distortion of the square planar CuO_4 unit was intentionally introduced to control absorption by both the charge transfer transition from O^{2-} to Cu^{2+} and the *d*–*d* transition of Cu^{2+}. The introduction of Li^+ into Cu^{2+} site caused not only the elongation of the local Cu–O distance which can shift the charge transfer absorption toward shorter wavelength but also the lowering of the symmetry of CuO_4 unit which is effective for increase of the *d*–*d* transition absorption and shift toward longer wavelength. Among the samples prepared, the $Ba(TiO)(Cu_{0.90}Li_{0.10})_4(PO_4)_4$ solid showed the highest blueness value ($b^* = -57.6$) and the hue angle ($H° = 268.7$) close to pure blue.

Chapter 2

Environmentally friendly inorganic blue pigments of $(Li_{1-x}Na_x)_2Cu_5(PO_4)_4$ solids were successfully prepared by a conventional solid-state reaction method. To decrease the *d*–*d* transition absorption in green region, larger size of Na^+ was introduced into the Li^+ site, which increased the *d*–*d* transition absorption with a shift to a longer wavelength. As a result of Na^+ doping, the absorption

in the green region at wavelengths from 520 to 560 nm was successfully increased. Among the samples prepared, a vivid blue color with the high blueness value (b^*= −39.4) was obtained for the $(Li_{0.90}Na_{0.10})_2Cu_5(PO_4)_4$ solid and it was found that this pigment possessed high durability for acid, heat, and UV irradiation.

Chapter 3

To investigate the effect of ionic radius and electronegativity of dopants on the coordination environment around Cu^{2+} together with new finding of candidate material for environmentally friendly inorganic blue pigment, $Na_4Cu_{1-x}M_x(PO_4)_2$ (M = Mg^{2+}, Ca^{2+}, Zn^{2+}) solids were synthesized. Comparing the solids prepared, it was found that the electronegativity of dopant also strongly affected the distortion of CuO_x units in the structure, and the $Na_4Cu_{0.85}Mg_{0.15}(PO_4)_2$ showed the highest blueness value (−b^*) of 38.2 owing to the elongation of Cu–O distance. From this result, it can be proposed that the distortion of CuO_x units by tuning the electronegativity of Cu^{2+} site is effective for improving blue hue of the pigments.

References

[1] *High Performance Pigments*, ed. by E.B. Faulkner, R.J. Schwartz, and Wiley-VCH, Weinheim, 2009. doi: 10.1002/9783527626915.

[2] *Industrial Inorganic Pigments*, ed. by G. Buxbaum and G. Pfaff, Wiley-VCH, Weinheim, 2005. doi:10.1002/3527603735.

[3] S. Faria and V. Chiora, *J. Electrochem. Soc.*, 1977, **124**, 623−625.

[4] V. Otero, L. Carlyle, M. Vilarigues, and M.J. Melo, *RSC Advances*, 2012, **2**, 1798−1805.

[5] G.E. Bacon and F.F. Robert, *Acta Crystallogr*., 1953, **6**, 57–62.

[6] V.S. Vishnu, G. George, and M.L.P. Reddy, *Dyes Pigm*., 2010, **85**, 117–123.

[7] L.S. Kumari, P.P. Rao, and P. Koshy, *J. Am. Ceram. Soc*., 2010, **93[5]**, 1402−1408.

[8] M. Llusar, L. Vitásková, P. Šulcová, M.A. Tena, J.A. Badenes, and G. Monrós, *J. Eur. Ceram. Soc*., 2010, **30**, 37−52.

[9] R.A. Candeia, M.I.B. Bernardi, E. Longo, I.M.G. Santos, and A.G. Souza, *Mater. Lett*., 2004, **58**, 569−572.

[10] P. Šulcová, L. Vitásková, and M. Trojan, *J. Therm. Anal. Calorim*., 2010, **99**, 409−413.

[11] P. Šulcová, P. Bystrzycki, L. Válek, and M. Trojan, *J. Min. Metall. Sect. B-Metall*., 2011, **47[2]B**, 105–112.

[12] G. George, V.S. Vishnu, and M.L.P. Reddy, *Dyes Pigm*., 2011, **88**, 109–115.

[13] P. Šulcová, J. Večeřa, and P. Bystrzycki, *J. Therm. Anal. Calorim*., 2012, **108**, 525−529.

[14] L. Stránská, P. Šulcová, and J. Mouchová, *J. Therm. Anal. Calorim*., 2012, **109**, 643−648.

[15] S.K. Biswas, D. Dhak, A. Pathak, and P. Pramanik, *Mater. Res. Bull*., 2008, **43**, 665–675.

[16] N. Pailhé, M. Gaudon, and A. Demourgues, *Mater. Res. Bull*., 2009, **44**, 1771–1777.

[17] V.S. Vishnu, G. George, V. Divya, and M.L.P. Reddy, *Dyes Pigm*., 2009, **82**, 53–57.

[18] V.S. Vishnu and M.L. Reddy, *Chem. Lett*., 2010, **39**, 820–821.

[19] L.S. Kumari, T.H. Gayathri, S.F. Sameera, and P.P. Rao, *J. Am. Ceram. Soc*., 2011, **94[2]**, 320−323.

[20] V.S. Vishnu, S. Jose, and M.L. Reddy, *J. Am. Ceram. Soc*., 2011, **94[4]**, 997–1001.

[21] P. Luňáková, M. Trojan, J. Luxová, and J. Trojan, *Dyes Pigm*., 2013, **96**, 264–268.

[22] G. George, G. George, P.P. Rao, and M.L. Reddy, *Chem. Lett*., 2005, **34**, 1702–1703.

[23] G. George, L.S. Kumari, V.S. Vishnu, S. Ananthakumar, and M.L.P. Reddy, *J. Solid State Chem*., 2008, **181**, 487–492.

[24] J.K. Kar, R. Stevens, and C.R. Bowen, *J. Alloys. Compd*., 2008, **455**, 121–129.

[25] T. Masui, A. Shiraishi, H. Nakado, N. Takeuchi, Wendusu, and N. Imanaka, *J. Jpn. Soc. Colour Mater.*, 2015, **88[7]**, 203−207.

[26] L.M. Schabbach, F. Bondioli, A.M. Ferrari, T. Manfredini, C.O. Petter, and M.C. Fredel, *J. Eur. Ceram. Soc*., 2007, **27**, 179−184.

[27] M. Dondi, F. Matteucci, G. Baldi, A. Barzanti, G. Cruciani, I. Zama, and C.L. Bianchi, *Dyes Pigm*., 2008, **76**, 179−186.

[28] S.W. Kim, Y. Saito, T. Hasegawa, K. Toda, K. Uematsu, and M. Sato, *Dyes Pigm*., 2017, **136**, 243−247.

[29] D. Saraswathy, P.P. Rao, S. Sameera, V. James, and A.K.V. Raj, *RSC Adv.*, 2015, **5**, 27278−27281.

[30] M. Ocaña, J.P. Espinós, and J.B. Carda, *Dyes Pigm*., 2011, **91**, 501–507.

[31] M. Llusar, A. Zielinska, M.A. Tena, J.A. Badenes, and G. Monrós, *J. Eur. Ceram. Soc*., 2010, **30**, 1887–1896 .

[32] D. Visinescu, C. Paraschiv, A. Ianculedcu, B. Jurca, B. Vasile, and O. Carp, *Dyes Pigm*., 2010, **87**, 125–131.

[33] A. Leite, G. Costa, W. Hajjaji, M.J. Ribeiro, M.P. Seabra, and J.A. Labrincha, *Dyes Pigm*., 2009, **81**, 211–217.

[34] Wendusu, T. Honda, T. Masui, and N. Imanaka, *Chem. Lett.*, 2013, **42**, 1562–1564.

[35] F. Funabiki, S. Matsuishi, and H. Hosono, *J. Phys. Chem. A*, 2011, **115**, 5081–5088.

[36] E. Kendrick, C.J. Kirk, and S.E. Dann, *Dyes Pigm.*, 2007, **73**, 13–18.

[37] C. Zhang, N. Zhang, X. Wang, and L. Zhang, *Mater. Res. Bull.*, 2018, **101**, 334–339.

[38] S. Jose and M.L. Reddy, *Dyes Pigm.*, 2013, **98**, 540–546.

[39] K. Kimura, M. Sera, and T. Kimura, *Inorg. Chem.*, 2016, **55**, 1002–1004.

[40] R.D. Shannon, *Acta Crystallogr. Sect. A*, 1976, **32**, 751–767.

[41] F. Izumi and K. Momma, *Sol. St. Phen.*, 2007, **130**, 15–20.

[42] L. Cui, S. Pan, J. Han, X. Dong, and Z. Zhou, *Solid State Sci.*, 2011, **13**, 1304–1308.

[43] A.W. Kolsi, *A. C. R. Seances Acad. Sci.*, 1977, **C284**, 483–486.

[44] A.L. Allred, *J. Inorg. Nucl. Chem.*, 1961, **17**, 215–221.

List of Publications

1. Novel Environment-Friendly Blue Pigments Based on $Ba(TiO)Cu_4(PO_4)_4$

Hiroaki Shirai, Shinji Tamura, Akihiro Miura, and Nobuhito Imanaka

Journal of the Japan Society of Colour Material, 2020, **93 (7)**, 214–218.

2. Novel Environmentally Friendly Blue Pigments Based on $Li_2Cu_5(PO_4)_4$

Hiroaki Shirai, Shinji Tamura, and Nobuhito Imanaka*

Ceramics International

in press.

3. Novel Environmentally Friendly Blue Pigments Based on $Na_4Cu(PO_4)_2$

Hiroaki Shirai, Shinji Tamura, and Nobuhito Imanaka*

Chemistry Letters

in press.

List of Supplementary Publications

1. Novel Photocatalyst Based on Metastable $ZrSnO_4$ Solid for Hydrogen and Oxygen Evolutions

Hiroaki Shirai, Naoya Akiyama, Naoyoshi Nunotani, and Nobuhito Imanaka*

Chemistry Letters, 2018, **47**, 723–725.

2. Photocatalytic Hydrogen Evolution from Water over Hafnium Oxyphosphate

Hiroaki Shirai, Naoyoshi Nunotani, and Nobuhito Imanaka*

Journal of the Ceramic Society of Japan, 2019, **127 (10)**, 700–702.

Acknowledgements

The author would like to express his heartfelt appreciation to Professor Dr. Nobuhito Imanaka, Department of Applied Chemistry, Graduate School of Engineering, Osaka University, for his continuous guidance, valuable suggestions, and his science encouragement throughout the work.

The author is indebted to Dr. Shinji Tamura, Department of Applied Chemistry, Graduate School of Engineering, Osaka University, for his continuous guidance and stimulating discussions for carrying out this work. The author is also very grateful to Dr. Naoyoshi Nunotani, Department of Applied Chemistry, Graduate School of Engineering, Osaka University, for his helpful suggestions and apposite advice.

The author would like to express his sincere gratitude to Professor Dr. Akinori Saeki and Professor Dr. Ken-ichi Nakayama, Department of Applied Chemistry, Graduate School of Engineering, Osaka University, for their constructive and valuable comments during the revision of this thesis.

The author also sends his appreciation to the Japan Society for the Promotion of Science for their financial support during the author's study.

Special thanks should be given to author's seniors and co-workers, Mr. Akihiro Miura, Mr. Yuji Hironaka, Dr. Bae Byungseo, Mr. Kenji Matsuo, Mr. Mizuki Momai, Mr. Takuya Kawaguchi, and Ms. Yo Shimura, for their helpful assistance and support in the course of this work, and the other members of the research group under direction of Professor Dr. Nobuhito Imanaka, Osaka University.

Finally, the author would like to extend deep gratitude to his parents, Mr. Hideki Shirai and Mrs. Wazumi Shirai, his younger brother, Mr. Tomotaka Shirai, and all members of his family for their encouragement, continuous understanding, and perpetual supports.